

Photoelectron imaging on vibrational excitation and Rydberg intermediate states in multi-photon ionization process of NH_3 molecule

Ya-Nan Sun(孙亚楠), Yan-Hui Wang(王艳辉), Le-Le Song(宋乐乐), Hai-Bin Du(杜海滨), Xiao-Chun Wang(王晓春), Lan-Lai He(赫兰海), Si-Zuo Luo(罗嗣佐), Qin Yang(杨钦), Jing Leng(冷静), Fu-Chun Liu(刘福春)

Citation: Chin. Phys. B . 2020, 29(9): 093201 . **doi:** 10.1088/1674-1056/ab9431
Journal homepage: http://cpb.iphy.ac.cn; http://iopscience.iop.org/cpb

What follows is a list of articles you may be interested in

Controlling Rydberg excitation process with shaped intense ultrashort laser pulses

Xiao-Yun Zhao(赵晓云), Chun-Cheng Wang(王春成), Shi-Lin Hu(胡师林), Wei-Dong Li(李卫东), Jing Chen(陈京), Xiao-Lei Hao(郝小雷)

Chin. Phys. B . 2019, 28(8): 083202 . **doi:** 10.1088/1674-1056/28/8/083202

Photoelectron imaging of resonance-enhanced multiphoton ionization and above-threshold ionization of ammonia molecules in a strong 800-nm laser pulse

Le-Le Song(宋乐乐), Ya-Nan Sun(孙亚楠), Yan-Hui Wang(王艳辉), Xiao-Chun Wang(王晓春), Lan-Hai He(赫兰海), Si-Zuo Luo(罗嗣佐), Wen-Hui Hu(胡文惠), Qiu-Nan Tong(佟秋男), Da-Jun Ding(丁大军), Fu-Chun Liu(刘福春)

Chin. Phys. B . 2019, 28(6): 063201 . **doi:** 10.1088/1674-1056/28/6/063201

Photoelectron angular distributions of H ionization in low energy regime: Comparison between different potentials

Shu-Na Song(宋舒娜), Hao Liang(梁昊), Liang-You Peng(彭良友), Hong-Bing Jiang(蒋红兵)

Chin. Phys. B . 2016, 25(9): 093201 . **doi:** 10.1088/1674-1056/25/9/093201

Lifetimes of Rydberg states of Eu atoms

Jing Hua, Ye Shi-Wei, Dai Chang-Jian

Chin. Phys. B . 2015, 24(1): 013203 . **doi:** 10.1088/1674-1056/24/1/013203

Field ionization process of Eu $4f^7 6snp$ Rydberg states

Zhang Jing, Shen Li, Dai Chang-Jian

Chin. Phys. B . 2015, 24(11): 113201 . **doi:** 10.1088/1674-1056/24/11/113201

Photoelectron imaging on vibrational excitation and Rydberg intermediate states in multi-photon ionization process of NH_3 molecule*

Ya-Nan Sun(孙亚楠)[1,4], Yan-Hui Wang(王艳辉)[2], Le-Le Song(宋乐乐)[1,3], Hai-Bin Du(杜海滨)[5], Xiao-Chun Wang(王晓春)[1,4], Lan-Lai He(赫兰海)[1,4], Si-Zuo Luo(罗嗣佐)[1,4], Qin Yang(杨钦)[1,4], Jing Leng(冷静)[1,4], and Fu-Chun Liu(刘福春)[1,4,†]

[1] *Institute of Atomic and Molecular Physics, Jilin University, Changchun* 130012, *China*
[2] *College of Electronic Science and Engineering, State Key Laboratory on Integrated Optoelectronics, Jilin University, Changchun* 130012, *China*
[3] *Jilin Institute of Chemical Technology, Jilin* 132022, *China*
[4] *Jilin Provincial Key Laboratory of Applied Atomic and Molecular Spectroscopy, Jilin University, Changchun* 130012, *China*
[5] *Department of Comprehensive, Harbin City Vocational College, Haerbin* 150000, *China*

(Received 31 March 2020; revised manuscript received 14 May 2020; accepted manuscript online 19 May 2020)

The ionization processes of NH_3 molecule are studied by photoelectron velocity map imaging technique in a linearly polarized 400-nm femtosecond laser field. The two-dimensional photoelectron images from ammonia molecules under different laser intensities are obtained. In the slow electron region, the values of kinetic energy of photoelectrons corresponding to peaks 1, 2, 3, and 4 are 0.27, 0.86, 1.16, and 1.6 eV, respectively. With both the kinetic energy and angular distribution of photoelectrons from NH_3 molecules, we can confirm that the two-photon excited intermediate Rydberg state is $A^{\sim 1}A_2''$ ($v_2' = 3$) state for photoelectron peaks 2, 3, 4, and the three peaks are marked as $1^2 2^3$ $(2+2)$, $1^1 2^3$ $(2+2)$, and $1^0 2^3$ $(2+2)$ multi-photon processes, respectively. Then, peak 1 is found by adding a hexapole between the source chamber and the detection chamber to realize the rotational state selection and beam focusing. Peak 1 is labeled as the $1^3 2^3$ $(3+1)$ multi-photon process through the intermediate Rydberg state $E^{\sim 1}A_1'$. The phenomena of channel switching are found in the slow electron kinetic energy distributions. Our calculations and experimental results indicate that the stretching vibrational mode of ammonia molecules varies with channels, while the umbrella vibration does not. In addition, we consider and discuss the ac-Stark effect in a strong laser field. Peaks 5 and 6 are marked as $(2+2+1)$ and $(2+2+2)$ above threshold ionization processes in the fast electron region.

Keywords: photoelectron velocity map imaging, photelectron angular distributions, Rydberg state, hexapole

PACS: 32.80.Rm, 32.60.+i, 32.80.Fb **DOI:** 10.1088/1674-1056/ab9431

1. Introduction

With the development of the ultra-fast laser pulse technique,[1] the ionization of atoms and molecules in intense laser fields have attracted considerable attention. The interactions between an ultra-fast laser and molecule produce many physical phenomena such as multi-photon ionization (MPI),[2] non-sequential double ionization (NSDI),[3] high-order harmonic generation (HHG),[4] and Coulomb explosion (CE).[5] The excited state dynamics of molecules can be studied by the MPI method and resonance-enhanced multi-photon ionization (REMPI) technique, which greatly contributes to the understanding of decay dynamics of excited states (usually Rydberg states).[6] In recent years, the use of a femtosecond laser to develop photoelectron velocity imaging has become a powerful tool for the detection of molecular MPI processes.[7,8] Li *et al.* have revealed the dynamics of the singlet state (s-1), the first excited state of o-dichlorobenzene, through using the time-of-flight mass spectrometric method and photoelectron velocity imaging technique.[9] We know that ionization process is an MPI process when the Keldysh coefficient is $r > 1$.[10] The MPI includes the above threshold ionization (ATI)[11] and REMPI.[12] During molecular ionization, dynamical information can be effectively obtained by detecting a photoelectron spectrum. However, molecular ionization is very complicated in a strong laser field. To better understand the ionization processes of molecules, we also need to extract angular distribution and kinetic energy distribution of photoelectrons from the photoelectron images.[13,14] For many years, NH_3 molecular ionizing processes have been widely investigated in a strong laser field.[15–18] NH_3 is a typical umbrella-type molecule, and the large amplitude of reversal motion makes its structure more complex than those of PH_3, SbH_3, and other molecules in the low frequency region. In 1978, Colson *et al.* studied the excited state dynamics of the NH_3 molecule for the first time. New electronic states of the NH_3 molecule were discovered by the $(2+2)$ REMPI technique.[19] In 2009, Paul Hockett *et al.* extracted the rotary-resolved photoelectron images through

*Project supported by the National Natural Science Foundation of China (Grant Nos. 11574116, 11534004, and 10704028).
†Corresponding author. E-mail: lfc@jlu.edu.cn
© 2020 Chinese Physical Society and IOP Publishing Ltd

multi-atomic ionization. The photoelectron angular distribution related to the formation of the NH_3 single rotating energy level has been extracted and analyzed.[20] In 2000, Xie *et al.* have used nanosecond and femtosecond lasers to study the resonance-enhanced multi-photon ionization (REMPI) photoelectron spectrum of NH_3 and also explained these multi-photon ionization (MPI) processes in detail.[17] In 2004, Meng *et al.* have confirmed that multi-photon process is a result of potential energy surface movement caused by the strong field effect according to time-dependent wave packet dynamics.[21] Then, the $E^{\sim}$ state of ammonia was also widely studied. The $E^{\sim 1}A_1'$ state of the NH_3 molecule was first identified by Colsonn *et al.* in the REMPI experiment[22] Ashfold *et al.* have used the two-photon REMPI of 275 nm–248 nm to further study the $E^{\sim 1}A_1'$ state.[23,24]

In our work, the ionization information about the NH_3 molecular beam is detected by velocity map imaging (VMI) in a strong femtosecond laser field at 400-nm wavelength. We extract the kinetic energy distributions (KEs) and photoelectron angular distributions (PADs) from the photoelectron images of NH_3 molecules according to different laser intensities. A 1-m-long hexapole is chosen to realize the rotational state selection and beam focusing. In the KEs of photoelectrons, we observe four peaks at 0.27, 0.86, 1.16, and 1.6 eV within the energy of a single photon from REMPI processes, and two peaks beyond the energy of a single photon (3.1 eV) are generated from ATI process. We further explain the REMPI and ATI process of the NH_3 molecule by analyzing the KEs and PADs of photoelectrons.

2. Experiment

In the experiment, we use a Ti:sapphire amplification laser system to generate a linearly polarized laser pulse with a central wavelength of 800 nm. The pulse width is 50 fs with the output energy of 4 mJ at the 1-kHz repetition rate. The polarization direction of the laser beam is parallel to VMI. We use BBO crystals to change the wavelength of the laser from 800 nm to 400 nm. Because the output of horizontally polarized laser is converted into vertical polarization by the BBO crystal, a half-wave plate is added to the output laser to make it horizontally polarized. We use a $\lambda/2$ wave plate and a Glan prism to adjust laser intensity. The laser intensity was calibrated by measuring the energy shifts of the non-resonant ATI peaks of Xe under the same experimental conditions. The range of laser energy is 1.01×10^{13} W/cm^2–1.01×10^{14} W/cm^2.

The experimental apparatus consists of a beam source chamber, a hexapole chamber, and a detector chamber. The molecular beam (1% NH_3 mixed in Ne) is ejected through the pulse valve in the beam source chamber, interacts with the electric field of the hexapole chamber, and finally reaches the detection chamber. The pulse valve repetition rate is 1000 Hz, and the pulse valve opening time is set to be 20 μs. In the experiment, laser beam is focused into the interaction zone of the detector through a convex lens with a focal length of 25 cm and interacts with the molecular beam. The resulting photoelectrons are accelerated by the repeller (R) and extractor (E) of the electrostatic lens system in the detection chamber and projected onto the dual-microchannel plate detector at the end of the flight. The photoelectron signal is recorded by a CCD camera connected to a computer, and the original photoelectric information is read and saved on the computer. The specification and equipment details of this experiment are described in Ref. [25].

3. Results and discussion

We calculate the vibrational energy values for the $X^{\sim}$ state of NH_3^+. Table 1 shows the vibrational energy levels obtained by the following equation[17] and from Ref. [26]:

$$E_{v_1v_2} = \omega_1(v_1+1/2)-\omega_1\chi_1(v_1+1/2)^2 + \omega_2(v_2+1/2)-\omega_2\chi_2(v_2+1/2)^2, \quad (1)$$

where $\omega_1 = 3376.6\ \mathrm{cm}^{-1}$, $\omega_1\chi_1 = 23\ \mathrm{cm}^{-1}$, $\omega_2 = 849.3\ \mathrm{cm}^{-1}$, and $\omega_2\chi_2 = 16\ \mathrm{cm}^{-1}$.

Table 1. In non-ponderomotive force case, values of energy needed for ammonia molecule to transform from the $X^{\sim}$ state to different vibration levels of (upper) A state and (lower) ammonia ion.

	NH_3 $(A^{\sim})v_2'$					
	$V_2'=0$	$V_2'=1$	$V_2'=2$	$V_2'=3$	$V_2'=4$	$V_2'=5$
Excitation energy/eV	5.73	5.83	5.95	6.06	6.17	6.29
	NH_3^+ $(X^{\sim})v_2$					
Ionization energy/eV	$V_2=2$	$V_2=3$	$V_2=4$	$V_2=5$		
$V_1=0$	10.64	10.73	10.82	10.91		
$V_1=1$	11.04	11.14	11.24	11.32		
$V_1=2$	11.46	11.55	11.64	11.73		
$V_1=3$	11.86	11.95	12.04	–		

Table 1 shows the calculation results of different vibration levels of the umbrella vibration mode v_2' in the excited state $A^{\sim}$ of NH_3, and the N–H stretching vibration v_1 and umbrella vibration v_2 in the $X^{\sim}$ state of NH_3^+. We use $v_1^n v_2^m$ to represent the continuous vibrational states, denoted as 1^n2^m, where n and m represent the vibrational quantum numbers. In the experiment, the energy of a single photon is 3.1 eV, the ionization energy of ammonia is 10.18 eV, and the total energy of four photons is 12.4 eV. Because the NH_3 ground state, intermediate state, and pre-dissociation state are from a similar geometric configuration, the $\Delta v = 0$ transition mainly

occurs. Using calculations, kinetic energy distributions, and angular distributions of photoelectrons from ammonia in this experiment, the multi-photon resonance ionization processes are shown in Fig. 1.

The processes, according to our calculation and experiment, are shown in Fig. 1. In the first three channels, molecules absorb 2 photons from the ground state to the A state and then absorb 2 more photons to the different energy levels of continuous state. In the last channel, molecules absorb 3 photons from the ground state to the E state and still absorb one more photon to the continuous state.

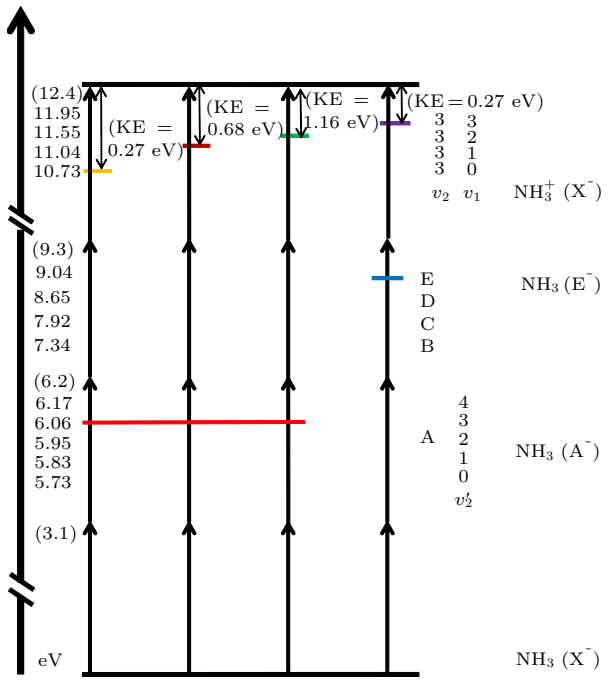


Fig. 1. Vibrational levels in different excited states of NH_3 and NH_3^+ without the existence of ponderomotive force potential. Single arrow represents the energy of a photon, and double arrow refers to the detected kinetic energy (KE) of electrons.

We measure the photoelectron velocity map images of the NH_3 molecule induced by a strong femtosecond laser. We choose neon as a carrier gas. The ionization energy of neon is 24.83 eV, and the ionization energy of NH_3 is 10.18 eV. Thus, carrier gas does not affect the molecules under investigation. There are no other ionic fragments in this laser range, which ensures that the electrons are ionized by the parent. Figure 2 shows two-dimensional photoelectron images of ammonia from REMPI and ATI processes.

Two completely different bright or dark ring structures are observed in two-dimensional photoelectron velocity images. The left-right asymmetry images in Fig. 2 are due to the efficiency of the detector. We rotate the detector, not including the CCD camera, 180° and perform the experiment again. By comparing two sets of images, the inverse efficiency effect between "left" or "right" half parts of the detector is obvious. In Figs. 2(a)–2(g), laser intensity varies from 1.01×10^{13} W/cm^2 to 3.8×10^{13} W/cm^2, and the images of photoelectrons are mainly due to the multi-photon resonance ionization processes of the NH_3 molecule. When laser intensity is relatively low, a bright ring structure near the center gradually disappears as laser intensity increases. This bright ring is defined as channel 1. The multiple bright ring structure, which is located far from the center, is clearly visible; we can define the inner ring as channels 2, 3 [they are distinguished as $1^2 2^3$ $(2+2)$ and $1^1 2^3$ $(2+2)$ multi-photon processes through energy calculations], and the outer ring as channel 4. With an increase in the laser intensity, it is observed that inner rings gradually become weaker and the outer rings become more enhanced, which occurs because the main photoelectron population converts from channels 2, 3 to channel 4. When the laser intensity varies from 3.8×10^{13} W/cm^2 to 1.01×10^{14} W/cm^2, the ATI gradually occurs, and the dark ring-like structure appears.

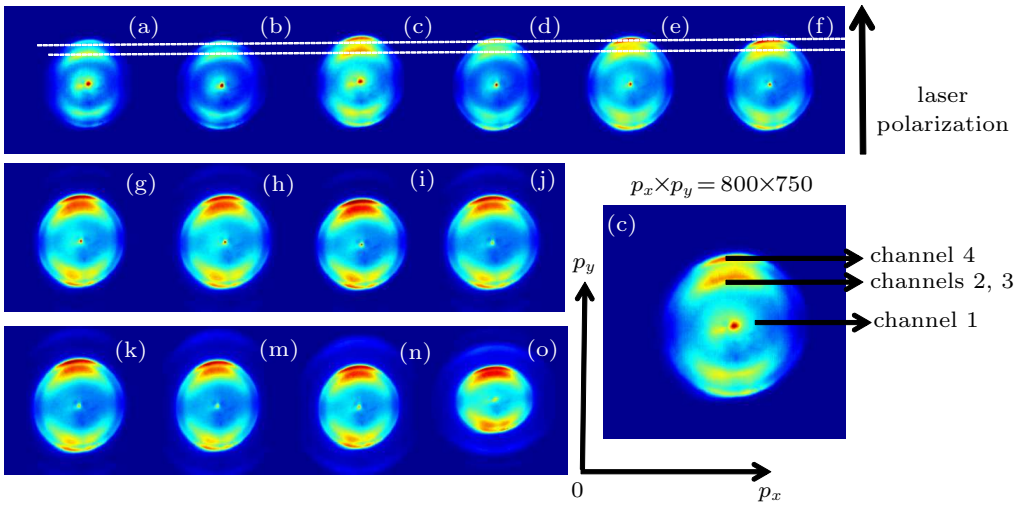


Fig. 2. Photoelectron images of NH_3 molecules. The laser wavelength is 400 nm, and the intensity range is 1.01×10^{13} W/cm^2–1.01×10^{14} W/cm^2. (a)–(n) Corresponding photoelectron distribution images with the laser intensity of 1.01, 1.27, 1.52, 1.90, 2.53, 3.17, 3.80, 4.43, 5.07, 5.70, 6.30, 7.60, 8.87, 10.10×(10^{13} W/cm^2). Horizontal and vertical coordinates are x and y pixels of CCD, respectively, and the direction of laser polarization is represented by arrows.

We extracted the KE values of photoelectrons from raw images, which are shown in Figs. 3 and 4. When the energy of a single photon is large, the molecular ionization processes corresponding to the slow electron region are relatively simple where the kinetic energy is less than the energy of a photon. In Fig. 3, there are four peaks. Peak 1 is observed only at the low laser intensity and disappears at the relatively high laser intensity. For peaks 2, 3, and 4, when the laser intensity increases, it is determined that peak 2 gradually weakens, peaks 3 and 4 gradually strengthen, and peak 4 finally becomes the most significant. This occurs because at high laser intensity, photoelectron population switches from channels 2 and 3 to channel 4. Finally, peak 4 becomes more pronounced and has the largest photoelectron population. This observation is consistent with the phenomenon shown in Fig. 2. Peaks 5 and 6 appear when the laser energy reaches the corresponding fast electron region as shown in Fig. 4. In fact, peak 6 is barely visible in Fig. 2 because it needs one more photon than peak 5 and two more photons than peak 4 to induce peak 6. Peak 5 is already much weaker than peak 4, and peak 6 is also weak. In addition, peak 6 is located in the cut of CCD images, and camera efficiency also becomes low.

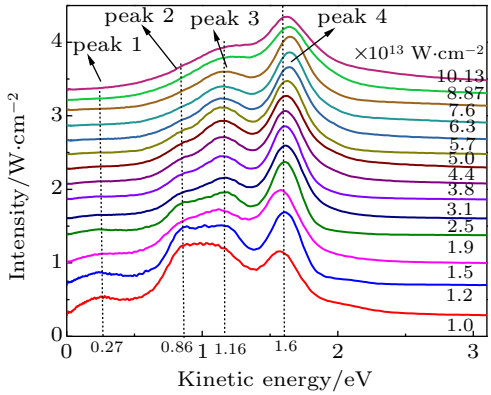


Fig. 3. Kinetic energy distributions from slow electrons within the range of 0 eV–3.1 eV with laser intensities being 1.0, 1.27, 1.52, 1.90, 2.53, 3.17, 3.80, 4.43, 5.07, 5.70, 6.30, 7.60, 8.87, and 10.1×(10^{13} W/cm^2).

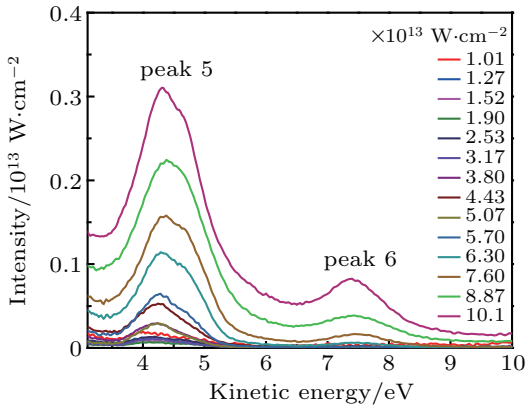


Fig. 4. Kinetic energy distributions of fast electrons within the range of 3.1 eV–10 eV with laser intensities being 1.01, 1.27, 1.52, 1.90, 2.53, 3.17, 3.80, 4.43, 5.07, 5.70, 6.30, 7.60, 8.87, and 10.1×(10^{13} W/cm^2).

Figure 3 shows that KE values of photoelectrons have four major peaks with the values of 0.27, 0.86, 1.16, and 1.6 eV, respectively. According to the NH_3^+ energy values of different vibration modes shown in Table 1, the corresponding four peaks are marked as 1^32^3, 1^22^3, 1^12^3, and 1^02^3, respectively. For example, for 1^02^3, which corresponds to peak 4, we use the energy of four photons minus the calculated energy of 1^02^3, which produces the final result of 1.67 eV; our experimental kinetic energy is 1.6 eV. Owing to the influence of the Stark shift, the energy values of the excited states and the continuous states vary at the same time; however, the ionization energy does not change. As shown in Fig. 3, the kinetic energy values of the four peaks corresponding to different laser intensities also remain basically unchanged. We know that the vibration modes of NH_3 ($A^\sim$) are umbrella bending long series. According to the Frank–Conton factor, the dominant vibration modes in the vibrational states of NH_3^+($X^\sim$) are also umbrella bending long series. Owing to the ac-Stark effect in a strong field,[27] the ponderomotive force potential (U_p) is generated, and U_p is proportional to the laser intensity I. Thus, the energy lines of Rydberg states move up with the increase in the laser intensity. The NH_3 molecule needs to absorb more photons to be ionized, and the extra photon energy absorbed, which is more than the ionization energy, will eventually be converted into the kinetic energy of the electron. Therefore, from Table 1, we can also calculate that the intermediate state 1^32^3 multi-photon process only exists in the case of low laser intensity, which ensures that the total energy is not greater than 12.4 eV when we add U_p to $E_{v_1v_2}$ (the value for 1^32^3 is 11.95 eV).

Peak 1 occurs because the NH_3 molecule absorbs three photons from the ground state to the excited states NH_3 ($E^\sim$) and then absorbs one more photon to the continuous state 1^32^3, which generates photoelectrons marked as the 1^32^3 $(3+1)$ resonance-enhanced multi-photon process (see Fig. 9), and the $(3+1)$-multi-photon processes are inhibited at high laser intensity. Peaks 2, 3, and 4 are derived from the resonance processes in which NH_3 molecules absorb two photons from the ground state to the excited NH_3 ($A^\sim$) $\nu_2' = 3$ states; then, photoelectrons are generated when NH_3 molecules take up two photons from the excited state to the reionization states of NH_3^+, which are $(2+2)$-resonance-enhanced multi-photon processes. The NH_3 from the ground state is excited to NH_3 ($A^\sim$) $\nu\,'_2 = 3$ when there is no ponderomotive force potential energy, which needs to absorb 6.06 eV. The ponderomotive force adds a minimum of 0.15 eV to the potential energy when laser intensity is 1×10^{13} W/cm^2. The $(2+2)$-REMPI processes have the same initial state and intermediate resonance state but different vibrational levels in the continuous states denoted as 1^22^3, 1^12^3, and 1^02^3. We know that 1^32^3, 1^22^3, 1^12^3, and 1^02^3 are different vibrational energy levels in the $X^\sim$ state of NH_3^+, which means that the N–H stretching mode moves

in the high frequency direction, while the umbrella mode does not change, because the ponderomotive force potential energy changes the potential energy surface of the ions along the N–H stretching direction. This stretching vibration effect causes switch among the NH_3 molecular ionization channels as seen from KEs; the peaks of 1^22^3 and 1^12^3 gradually weaken, and the peak value of 1^02^3 gradually increases with laser intensity increasing.

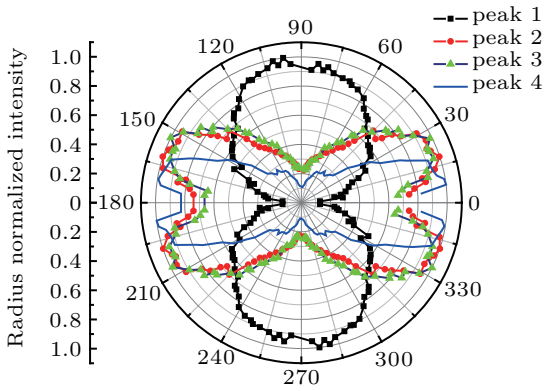


Fig. 5. Angular distributions of peaks 1, 2, 3, and 4, corresponding to 1.01×10^{13} W/cm^2 laser intensity.

To clearly identify the multi-photon processes corresponding to the four peaks in the low energy region, it is necessary to extract the angular distributions from original images. In Fig. 5, the angular distribution of peak 1 differs from those of peaks 2, 3, and 4; thus, the intermediate state of peak 1 is inconsistent with the intermediate state of other peaks. In addition, in the range of laser intensities, our measurements show that the ponderomotive force potential (U_p) varies from 0.15 eV to 1.5 eV. Because the minimum energy of Rydberg state E without an external field is 9.04 eV, the three photon energy values are all 9.3 eV; ammonia molecules are excited directly into the E-state at low laser intensity. Peak 1 should be a multi-photon process so that the ammonia molecule absorbs 3 photons to reach the intermediate Rydberg state of E$^{\sim}$ and then absorbs 1 photon to reach the continuous state. In addition, the lifetime of A$^{\sim}$ Rydberg state is on a femtosecond scale and that of E$^{\sim}$ is on a picosecond scale; thus, E is more stable. With the increase in the laser intensity, owing to the influence of U_p, the energy of the E Rydberg state is greater than 9.3 eV, and three photons can no longer excite the molecule to the E Rydberg state; thus, the channel is closed. In addition, the continuous state moves to the ionization off-line of NH_2 under the influence of U_p, and NH_3^+ will further dissociate into NH_2 (the IP of NH_2 is 12.0 eV);[28,29] thus the channel of peak 1 disappears. This is consistent with the observed phenomenon in the images. All above mentioned results and analyses confirm that peak 1 should be marked as the $(3+1)$ process rather than the $(2+2)$ process. Moreover, we can observe peak 1 when a hexapole is used to focus the molecular beam, and electrons with small kinetic energy are also detected. The hexapole generates an inhomogeneous electrostatic field; thus, one can realize rotational state selection and molecular beam focusing. In the experiment, a relatively pure $|222\rangle$ state can be obtained when the hexapole voltage is 7.8 kV, and a five-time signal enhancement is achieved through beam focusing. The detailed references are available in our previous work.[30,31]

Compared with the existing experimental results,[17] peaks 2, 3, and 4 should be $(2+2)$-MPI processes; specifically, the ammonia molecule absorbs 2 photons and is excited to an intermediate state (A$^{\sim}$ Rydberg state) and then again absorbs 2 photons to reach the continuous state. Moreover, the angular distributions of the three peaks are basically consistent, which indicates that neither the initial state nor the A$^{\sim}$ intermediate state changes, and only the reached continuous states are different. Figure 6 shows that the maximum values of peak 4' PADs gradually change from approximately 28° or 152° to approximately 20° or 160° with laser intensity increasing. This observation indicates that laser intensity has almost no effect on angular distribution; only the potential energy of the intermediate state slightly changes under the action of an external field, and the orbits become slightly wider.

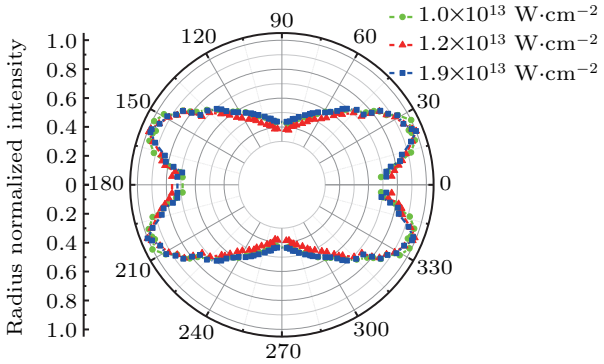


Fig. 6. Angular distributions of peak 4 at different laser intensities.

Peaks 5 and 6 originate from ATI processes; electron kinetic energy peaks are formed by absorbing one more photon and two more photons, which are denoted as $[(2+2)+1]$ process and $[(2+2)+2]$ process, respectively. ATI is characterized by the appearance of similar electron peaks in the photoelectron spectrum approximately one photon energy position apart. It is observed that the more the adsorbed photons is and the stronger the laser field becomes, the smaller the electronic signal is and the greater the proportion of obtained ATI is in the total electrical signal. This is the inevitable result of MPI process. In addition, one cannot distinguish discrete peaks, which results in the multiple peaks being superimposed mutually. At the same time, an electron correlation effect appears with laser intensity increasing, and the interference between

electrons also leads the peak 5; 1^22^3, 1^12^3, and 1^02^3 to be superimposed together, forming a large peak, and so does peak 6.

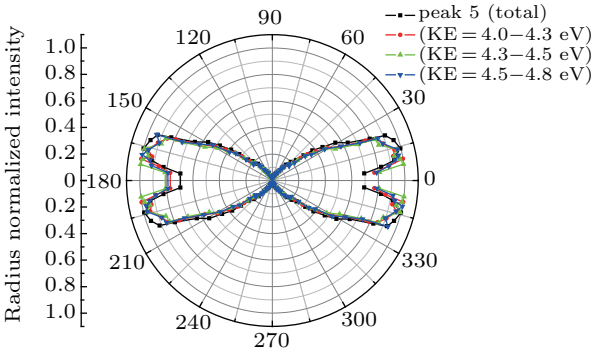


Fig. 7. Angular distribution of peak 5 at laser intensity 5.07×10^{13} W/cm^2.

According to the existing experimental results,[17] peak 5 should be contributed to from three discrete vibrational excitation processes. The energy distribution is from 4.0 eV to 4.8 eV, which is slightly over the sum of peaks 2, 3, and 4. However, we do not obtain discrete peaks' structure in Fig. 3. Nevertheless, we still provide the angular distributions of different values of kinetic energy in the case of discrete peaks as shown in Fig. 7 because those are mentioned in Ref. [17]. Thus, we observe that their angular distributions are almost the same as those of peaks 2, 3, and 4. Then, we compare the angular distribution of peak 4 with those of peaks 5 and 6 in Fig. 8. The angular distributions of peaks 4 and 5 are only slightly different, which confirms that our result for peak 5 is a sum of 1^22^3, 1^12^3, and 1^02^3 processes, and the three processes are superposed together to form a large peak. We know that the photoelectrons from ATI processes interfere with each other;[12] thus, we cannot experimentally obtain 1^22^3, nor 1^12^3, nor 1^02^3 splitting peak.

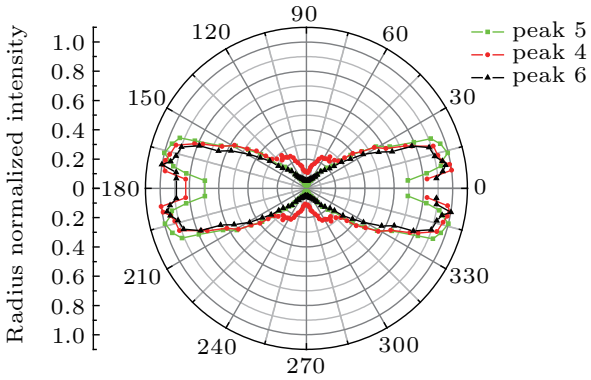


Fig. 8. Angular distribution of peaks 4, 5, and 6 at the 5.07×10^{13}-W/cm^2 laser intensity.

Finally, figure 9 clearly shows that the multi-photon process of ammonia in the strong femtosecond 400-nm wavelength laser field is divided into four parts, *i.e.*, (3 + 1), (2 + 2), (2 + 2 + 1), and (2 + 2 + 2). The peaks are also denoted as 1^32^3, 1^22^3, 1^12^3, and 1^02^3 vibrational mode; and the angular distributions of different intermediate states are also given in the REMPI region and ATI region.

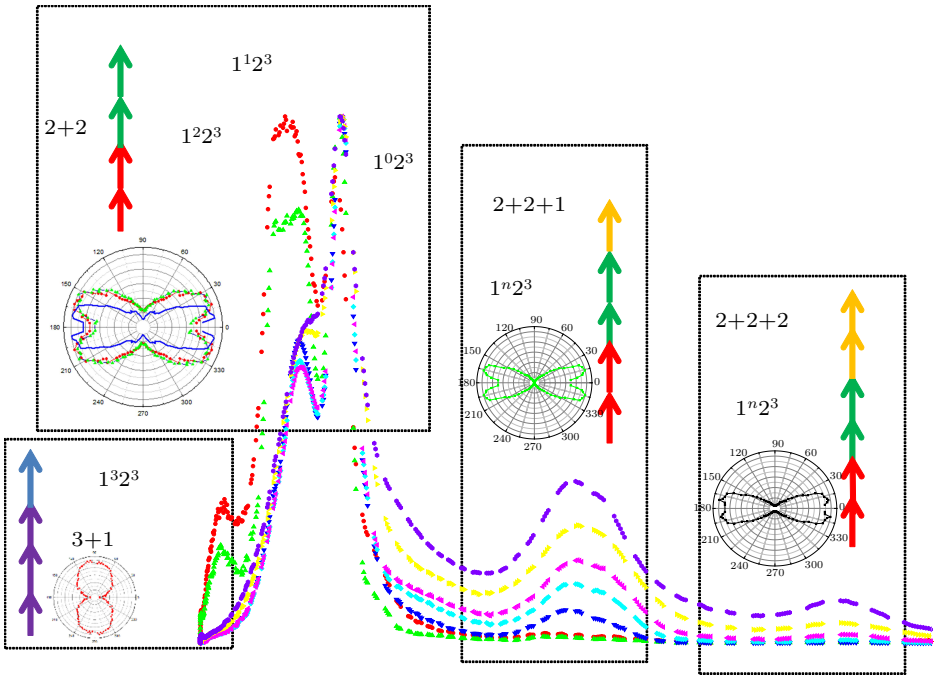


Fig. 9. Results and identification for multi-photon processes of ammonia in the 400-nm wavelength laser field. Colored arrows in this picture illustrate different multi-photon processes; all photons have the 400-nm wavelength.

4. Conclusions

In this work, the photoelectron velocity imaging technique is used to detect the photoelectron energy spectrum of NH_3 molecules at the 400-nm laser wavelength, and the KEs and PADs are extracted from photoelectron images. The REMPI process of NH_3 (3 + 1) or (2 + 2), and the ATI pro-

cesses of NH_3 $(2+2+1)$ and $(2+2+2)$ are fully analyzed. In kinetic energy distributions, we observe four peaks in the slow electron region and perform the identification of them. The results show that the stretching vibration of the molecule changes but the umbrella vibration does not. By comparing the photoelectron images with kinetic energy spectra at different laser intensities, the channel switching of quantum states is observed. By observing the variations of REMPI photoelectron peaks under different laser intensities, the effectiveness of channel switching is further confirmed. The KE lies in the more than one photon region where the photoelectrons originate from ATI processes, and the corresponding peaks appear. In addition, we provide a simple description for these processes. The photoelectron velocity images produced by the interaction of femtosecond laser with molecules are experimentally studied. The influence of laser intensity on the resonance excitation ionizing paths is analyzed, and the contribution of different Rydberg states to ionization processes is discussed. The kinetic energy and angular distributions of photoelectrons are analyzed to provide experimental basis for further understanding the ionization processes of molecules. Because there is a hexapole device in the laboratory that can select and focus molecules[32] and the laser alignment technique is used, highly aligned molecules can be used for further photoelectric imaging detection. The combination of the pump–probe technique or the two-color field method can improve time resolution and energy resolution, which serves as a foundation for the further analysis of intra-molecular orbital effects.[33–35]

References

[1] Popmintchev T 2013 *Am. Assoc. For Advancement Sci. Annu. Meeting Hynes Convention Center*, February **17**

[2] Kulander K C 1987 *Phys. Rev. A* **35** 445

[3] Fittinghoff D N, Bolton P R and Chang B 1992 *Phys. Rev. Lett.* **69** 2642

[4] Ganeev R A 2009 *Phys-usp+* **52** 65

[5] VagerZ, Naaman R and Kanter E P 1989 *Science* **244** 426

[6] Ashfold M N R, Langford S R, Morgan R A, Orr-Ewing A, Western C, Scheper C and De Lange C 1998 *Eur. Phys. J. D* **4** 189

[7] Li M, Zhang P, Luo S, ZhouY, Zhang Q B, Lan P F and Lu P X 2015 *Phys. Rev. A* **92** 063404

[8] Oppermann M, Weber S J and Frasinski L J 2013 *Phys. Rev. A* **88** 043432

[9] Yuan L W, Wang Y Q and Li W 2004 *Sci. China- Chem.* **47** 283

[10] Tang Y, Suzuki Y, Horio T and Suzuki T 2010 *Phys. Rev. Lett.* **104** 073002

[11] Agostini P, Fabre F, Mainfray G, Petite G and Rahman N K 1979 *Phys. Rev. Lett.* **42** 1127

[12] Song L L, Sun Y N, Wang Y H, Wang X C, He L H, Luo S Z, Hu W H, Tong Q N Ding D J and Liu F 2019 *Chin. Phys. B* **28** 063201

[13] Cooper J and Zare R N 1968 *J. Chem. Phys.* **48** 942

[14] Wu J, Schmidt L, Kunitski M, Meckel M, Voss S, Sann H, Kim H, Jahnke T, Czasch A and Dörner R 2012 *Phys. Rev. Lett.* **108** 183001

[15] Paul H, Katharine L R and MichaelS 2010 *Mol. Phys.* **108** 1045

[16] BieSuer J, Schnieder L, Schnieder J, *et al.* 1988 *J. Chem. Phys.* **88** 3607

[17] Xie J, Jiang B, Li G, Yang S, Xu J, Sha G, Xu D, Lou N and Zhang C 2000 *Faraday Discuss* **115** 127

[18] Rodríguez J D, González M G, Rubio L L and Banares L 2014 *Phys. Chem. Chem. Phys.* **16** 3757

[19] Nieman G C and Colson S D 1978 *J. Chem. Phys.* **68** 5656

[20] Hockett P, Staniforth M, Reid K L and Townsend D 2009 *Phys. Rev. Lett.* **102** 253002

[21] Meng Q T and Han K L 2004 *J. Atom. Mol. Phys.* **B04** 260

[22] Glownia J H, Riley S J, Colson S D and Nieman G C 1980 *J. Chem. Phys.* **73** 4296

[23] Ashfold M N R, Western C M, Hudgens J W and Johnson R D 1996 *Chem. Phys. Lett.* **260** 27

[24] Ashfold M N R, Dixon R N and Stickland R J 1984 *Chem. Phys.* **88** 463

[25] Luo S Z, Zhu R H, He L H, Hu W, Li X, Ma P, Wang C C, Liu F C, Roeterdink W G, Stolte S and Ding D J 2015 *Phys. Rev. A* **91** 053408

[26] Evans N L, Yu H, Roberts G M, Stavros V G and Ullrich S 2012 *Phys. Chem. Chem. Phys.* **14** 10401

[27] Bennewitz H G, Paul W and Schlier C Z 1955 *Physik* **141** 6

[28] Dunlavey S J, Dyke J M, Jonathan N and Morris A 1980 *Mol. Phys.* **39** 1121

[29] Locht R, Servais C, Ligot M and Momigny J 1988 *Chem. Phys.* **123** 443

[30] Liu F C, Jin M X, Gao X and Ding D J 2006 *Chin. Phys. Lett.* **23** 344

[31] Liu F C, Jin M X and Ding D J 2006 *Chin. Phys. Lett.* **23** 1165

[32] Song L L, WangY H, Wang X C, Sun H T, He L H, Luo S Z, Hu W H, Li D X, Zhu W H, Sun Y N, Ding D J and Liu F C 2019 *Chin. Phys. B* **28** 023101

[33] Mcfarland B K, Farrell J P, Bucksbaum P H and Gühr M 2008 *Science* **322** 1232

[34] Farrell J P, Petretti S, Förster J, McFarland B K, Spector L S, Vanne Y V, Decleva P, Bucksbaum P H, Saenz A and Gühr M 2011 *Phys. Rev. Lett.* **107** 083001

[35] Ohmura H and Nakanaga T 2004 *J. Chem. Phys.* **120** 5176